Ninth Fuel and Combustion Conference of Iran
Feb. 8 - 10, 2022, Shiraz University, Shiraz, Iran
FCCI-2022-0078

Combustion characteristics of premixed H_2-air in wavy microchannels for micro thermophotovoltaic applications

Pouyan Abbaspour[1], Alireza Alipoor[2*]
1- Department of Mechanical Engineering, Shahid Chamran University of Ahvaz, Ahvaz, Iran, pouabbaspour@gmail.com
2-School of Mechanical Engineering, Shiraz University, Shiraz 71348-51154, Iran, a.alipoor@shirazu.ac.ir
*Corresponding author

Abstract
Combustion characteristics of premixed H_2-air numerically investigated in wavy wall microchannels to examine the ability of such geometries to use as the heat source of a micro thermophotovoltaic system. Effect of inlet velocity, wall wave number, wave amplitude, and wall thermal conductivity studied by calculation of wall and fluid temperatures and the system's total efficiency. According to the results, wall temperature increases by inlet velocity enhancement due to flame stretch and flame transfer towards the concave areas contrived in the walls, whereas total efficiency of the system decreases due to fuel consumption increasement. It was found that when the number of waves enhances up to 10, the total efficiency of the system rises 74% in comparison with the similar flat wall microchannel. Moreover, wavy walls showed good thermal performance when heat recirculation increased by wall thermal conductivity. It caused to increase average wall temperature and the total efficiency accordingly. Finally, the results showed acceptable potential of wavy microchannels for usage in the micro thermophotovoltaic systems.
Keywords: Wavy wall microchannel, Hydrogen, Emitter efficiency, Heat recirculation

Introduction

Micro thermophotovoltaic (MTPV) systems have increased attention due to their advantages over traditional chemical batteries. An array of photovoltaic cells in the vicinity of a heat source (or thermal emitter) can convert thermal energy to electricity, which can be used as a power source of portable micro-electro-mechanical systems (MEMS). Although the batteries have been the only sources of power in portable MEMS for years, today, demand for small, light-weight, fast-charging, and high voltage power sources have challenged their usage. It has led to the development of micro combustion chambers as heat sources of the MTPV systems. Because of the exothermic reaction and high surface-to-volume ratio of micro combustion chambers, energy density is high enough to be worth paying more attention to. In addition, micro combustion chambers can better adapt to size reduction. For instance, even if we use a micro combustor as a heat source with an energy converter of 10% efficiency, the scale of the power system can be reduced to one-tenth the size of conventional chemical batteries [1]. As a practical example, a prototype of a microtube combustor of 0.113 m^3 in volume developed by Yang et al. [2] succeeded in delivering electrical power output of 0.92 W, as it was contrived in a MTPV power generator with a GaSb photovoltaic cell array. However, miniaturization of combustion chambers has challenges due to the high level of heat flux, inadequate residence time for complete combustion, and even flame-wall interaction, which may be the leading cause of blow-off, instabilities, and quenching phenomena. These challenges caused some innovations to be born to improve micro combustors performance and flexibility. Yang et al. [3] examined microtubes with a backward-facing step to prolong flow residence time. Vortexes generated due to the backward-facing step, had an important effect on the flame location and let the micro combustion chamber examine higher mass flow rates without blow-off. Yang et al. [3] showed that increasing the backward-facing step's height could raise the maximum output power of the system. An experimental study on the wall temperature and radiation heat flux of cylindrical micro combustors with a backward-facing step was carried out by Li et al. [4]. They found that the optimum efficiency was achieved at equivalence ratio of 0.8 for premixed H_2-air, independent of the combustor's diameter, length, and flow velocity, if the micro combustor worked as an emitter. Fan et al. [5] investigated a micro combustor with a bluff body. The recirculation zone behind the bluff body increases flow time, also it can store released heat of combustion. They showed as the thermal conductivity of material increases, more heat is transferred to upstream walls, and the incoming mixture is preheated better. Therefore, the gaseous volume expands more dramatically, which leads to a smaller low-velocity zone behind the bluff body. Hence, the blow-off limit becomes more limited. In the following, Fan et al. [6] followed their study by investigating bluff-body shape. They demonstrated that the triangular bluff body has a smaller blow-off limit than the semicircular one because of the stronger flame stretch caused by shear layers. Ansari and Amani [7] investigated a micro combustor with a bluff body and baffle. They showed that the efficiency of the system decreases in the absence of the baffle, and the flame is not stable at some conditions in the absence of the bluff body. Akhtar et al. [8] showed that stepped micro combustors with

trapezoidal and triangular cross-sections had higher efficiency when used as a heat source in the MTPV systems. Qian et al. [9] numerically investigated the performance of a MTPV system with a porous wall and bluff body. The system succeeded in attaining maximum total efficiency of 9.41%. Zuo et al. [10] showed that making a cavity in the microtube combustors caused to rise thermal performance of the micro combustor for MTPV applications. Because it has positive effects on reducing the nonuniformity of the outer wall temperature. Alipoor et al. [11] numerically investigated performance of a radial micro combustor by premixed H_2-air mixture. They found that generated vortexes are suitable for intensifying reactions in the radial part of the micro combustor. Their system achieved maximum total efficiency of 3.14% at equivalence ratio of 0.8. Recently, more complex geometries such as counter flow double-layer four-channel micro combustors [12], U-shaped microtubes [13], microtube with internal micro-fin [14] and multi-channel micro combustors [15] are investigated and researches are still ongoing. Their purpose is to achieve high and uniform wall temperature distribution while less fuel consumption. Combustion characteristics of premixed methane-air in wavy wall microchannels with heated walls investigated by Mansouri [16]. It was found that wall temperature enhancement moves the flames towards the inlet, whereas the flame moves towards the outlet by wave number enhancement. Mansouri [17] followed investigations by calculation of emitter efficiency and found that wavy walls increase the emitter efficiency by 8.3% compared to flat walls. Despite the superiority of hydrogen over other hydrocarbon fuels, investigation of hydrogen combustion characteristics in wavy microchannels is missed in the previous research. While hydrogen has advantages, including higher heating value and low emission. Also, the effects of the wall's wave amplitude and thermal conductivity have not been considered in the existing literature. With this motivation, combustion characteristics of premixed H_2-air numerically investigated in the present work with the effect of wall parameters containing thermal conductivity, the amplitude of waves, the number of waves, and inlet velocity on the MTPV efficiency.

Governing Equations

Governing equations consist of continuity, momentum, species conservation, energy, and ideal gas law, which drove as steady state. Turbulent flow regime is assumed, and the Realizable $K-\epsilon$ model is chosen for turbulence model because this model is better for rotation, strong adverse pressure gradients, recirculation, mixing, and channel flows [18]. Governing equations are presented by equations (1) to (6). For the symbols used in the equations, see the list of symbols following the conclusions section.

Continuity:

$$\frac{\partial(\rho u_i)}{\partial x_i} = 0 \tag{1}$$

Momentum:

$$\frac{\partial(\rho u_i u_i)}{\partial x_i} = -\frac{\partial P}{\partial x_i} + \frac{\partial}{\partial x_i}\left(-\frac{2}{3}\mu\frac{\partial u_k}{\partial x_k}\delta_{ij} + \mu\left(\frac{\partial u_i}{\partial x_j}+\frac{\partial u_j}{\partial x_i}\right)\right) \tag{2}$$

Energy in the fluid:

$$\frac{\partial(\rho u_i h)}{\partial x_i} = -\frac{\partial}{\partial x_i}\left(K_f\frac{\partial T}{\partial x_i}\right) + \frac{\partial}{\partial x_i}\left(\rho\sum_{k=1}^{N} h_k Y_k V_{k,i}\right) + \sum_{i=1}^{N} h_i\dot{\omega}_i \tag{3}$$

Species conservation equation:

$$\frac{\partial(\rho u_i Y_i)}{\partial x_i} = \frac{\partial}{\partial x_i}\left(\rho D_{i,m}\frac{\partial Y_i}{\partial x_i}\right) + \dot{\omega}_i \tag{4}$$

Ideal gas equation of state:

$$P = \rho\frac{R_u}{\overline{W}}T \tag{5}$$

Energy in the solid region:

$$\frac{\partial}{\partial x_i}\left(k_s\frac{\partial T}{\partial x_i}\right) = 0 \tag{6}$$

Where K_s is wall thermal conductivity. $D_{i,m}$ is the average mass diffusivity of the i^{th} species and calculated as [19].

$$D_{i,m} = \frac{1-x_i}{\sum_{j\neq i}\left(\frac{x_i}{D_{ij}}\right)} \tag{7}$$

Chapman-Enskog relation [19] is used to calculate the binary diffusion coefficient D_{ij} as follows:

$$D_{ij} = 10.1325\frac{0.001858T^{1.5}(W_{ij})^{-0.5}}{p\sigma_{ij}{}^2\Omega_D} \tag{8}$$

$$\sigma_{ij} = \frac{\sigma_i+\sigma_j}{2} \quad ; \quad W_{ij} = \left(\frac{1}{W_i}+\frac{1}{W_j}\right)^{-1}$$

$$\Omega_D = \frac{1.06036}{T_N{}^{0.15610}} + \frac{0.193}{\exp(0.47635T_N)} + \frac{1.03587}{\exp(1.52996T_N)} + \frac{1.76474}{\exp(3.89411T_N)}$$

$$T_N = \frac{T}{E_{ij}} \quad ; \quad E_{ij} = \frac{\varepsilon_{ij}}{k_B} \quad ; \quad \varepsilon_{ij} = \left(\sqrt{\varepsilon_i \varepsilon_j}\right)$$

Transport equations for the Realizable K-ε model are [18];

$$\frac{\partial}{\partial x_j}(\rho k u_j) = \frac{\partial}{\partial x_j}\left[\left(\mu + \frac{\mu_t}{\sigma_k}\right)\frac{\partial k}{\partial x_j}\right] + G_k + G_b - \rho\varepsilon - Y_M + S_k \quad (9)$$

$$\frac{\partial}{\partial x_j}(\rho \varepsilon u_j) = \frac{\partial}{\partial x_j}\left[\left(\mu + \frac{\mu_t}{\sigma_\varepsilon}\right)\frac{\partial \varepsilon}{\partial x_j}\right] + \rho C_1 S\varepsilon - \rho C_2 \frac{\varepsilon^2}{k + \sqrt{v\varepsilon}} + C_{1\varepsilon}\frac{\varepsilon}{k} C_{3\varepsilon} G_b + S_\varepsilon \quad (10)$$

Where,

$$C_1 = \max\left[0.43, \frac{\eta}{\eta + 5}\right], \quad \eta = S\frac{k}{\varepsilon}, \quad S = \sqrt{2 S_{ij} S_{ij}}, \quad S_{ij} = \frac{1}{2}\left(\frac{\partial u_j}{\partial x_i} + \frac{\partial u_i}{\partial x_j}\right) \quad (11)$$

And turbulent viscosity is calculated as:

$$\mu_t = \rho C_\mu \frac{k^2}{\varepsilon} \quad (12)$$

C_μ is no longer constant and it is computed from:

$$C_\mu = \frac{1}{A_0 + A_s \frac{k U^*}{\varepsilon}}, \quad U^* = \sqrt{S_{ij} S_{ij} + \tilde{\Omega}_{ij} \tilde{\Omega}_{ij}} \quad (13)$$

$$\tilde{\Omega}_{ij} = \Omega_{ij} - 2\varepsilon_{ijk}\omega_k$$

$$\Omega_{ij} = \overline{\Omega}_{ij} - \varepsilon_{ijk}\omega_k$$

$$A_0 = 4.04, \quad A_s = \sqrt{6}\cos\emptyset$$

$$\emptyset = \frac{1}{3}\cos^{-1}(\sqrt{6}\, W), \quad W = \frac{S_{ij} S_{jk} S_{ki}}{\tilde{S}^3}$$

$$\tilde{S} = \sqrt{S_{ij} S_{ij}}, \quad S_{ij} = \frac{1}{2}\left(\frac{\partial u_j}{\partial x_i} + \frac{\partial u_i}{\partial x_j}\right)$$

Where $\overline{\Omega}_{ij}$ is the mean rate of rotation tensor viewed in a moving reference frame with the angular velocity ω_k.

Three kinds of efficiency, named as energy conversion efficiency (η_Q), emitter efficiency (η_{Rad}), and total energy conversion efficiency of the MTPV system (η_{total}), were defined as Eqs. (14)-(19) [13], respectively. The heat loss (convection and radiation) ratio to the chemical heat release rate is defined as the energy conversion efficiency.

$$\eta_Q = \frac{\dot{Q}_w}{\dot{Q}_R} \quad (14)$$

Where $\dot{Q}_w$ and $\dot{Q}_R$ are total heat loss rate from the external wall and chemical heat release rate, respectively. These are defined as:

$$\dot{Q}_w = \sigma\epsilon A(T_w^4 - T_{surr}^4) + h_{conv} A(T_w - T_{surr}) \quad (15)$$

$$\dot{Q}_R = \dot{m}_{H_2} Q_{LHV} \quad (16)$$

Where T_w and T_{surr} are wall temperature and surrounding temperature, respectively. $\dot{m}_{H_2}$ is the mass flow rate of the hydrogen. Also, the lover heating value of the hydrogen, Q_{LHV} is considered to be 119 MJ/Kg [19]. The ratio of the radiation heat transfer rate from the outer surfaces of the micro combustion chamber ($\dot{Q}_{Rad}$) to the chemical heat release rate ($\dot{Q}_R$) is defined as the emitter efficiency (η_{Rad}).

$$\eta_{Rad} = \frac{\dot{Q}_{Rad}}{\dot{Q}_R} \quad (17)$$

Where,

$$\dot{Q}_{Rad} = \sigma\epsilon A(T_w^4 - T_{sur}^4) \quad (18)$$

The total energy conversion efficiency of the MTPV system (η_{Total}) is calculated by multiplying the emitter efficiency (η_{Rad}) and MTPV array efficiency (η_{MTPV}) as:

$$\eta_{Total} = \eta_{Rad}\eta_{MTPV} \quad (19)$$

MTPV array efficiency (η_{MTPV}) is defined as the conversion of the radiation energy to electrical energy. Its value is assigned to be 15% [13].

Geometry, Boundary Conditions, and Numerical Approach

A set of two-dimensional wavy microchannels were chosen for the geometry, and their schematic diagrams were illustrated in Figure 1(a). All of them have 45 mm long and 2 mm in channel width. Inner walls are chosen wavy because it helps to promote absorption of released heat due to surface enhancement, whereas outer walls are considered flat. Waves of the inner walls were designed based on a profile that is presented by Eq (20). In order to focus on geometry aspects, two parameters a and b were defined in the equation of the internal wall profile. The parameter a denotes amplitude of waves, b denotes the number of waves, and the geometries are categorized by them in Figure 1(b). Also, the minimum thickness of the wall is considered 0.8 mm for all cases.

$$y = aCos(2\pi b/L) \quad (20)$$

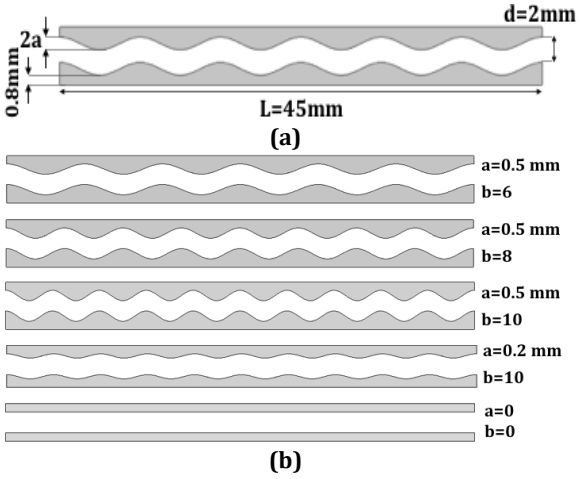

Figure 1: Dimensions and defined geometrical parameters (a), microchannels which categorized based on defined geometrical parameters

Regarding the boundary conditions, uniform inlet velocity and zero-gradient pressure are applied at the inlet where premixed H_2-air is entered at the temperature of 300 K and equivalence ratio of 0.8. No-slip boundary condition for velocity and zero-gradient boundary condition for pressure and species mass fractions are considered at the inner walls. Also, coupled condition is assumed for the temperature at the fluid-wall interface. Mixed conditions (convection and radiation) are considered at the outer walls. Surrounding temperature and convection heat transfer coefficient were set to 300 K and 10 $W/m^2.K$, respectively based on the existing literature [20]. Thermal radiation emissivity of the wall and thermal conduction coefficient of the wall is determined according to the wall material where Quartz and Silicon Carbide were considered as the wall materials, and their thermal properties are reported in Table 1. Pressure-outlet boundary condition is imposed at the outlet where the outlet pressure is assumed 1atm. In order to initiate the combustion process and activate reactions, the initial temperature is set to 2000 K for both fluid and solid zones. This should not affect numerical results because of steady state condition. The second-order upwind scheme and SIMPLE algorithm were considered for the governing equations discretization and coupling of the pressure-velocity fields, respectively. Also, residuals were set to 10^{-6} for convergence criterion. Surface reactions were neglected, and Discrete Ordinate (DO) model was set for surface-to-surface thermal radiation. Governing equations were solved in two-dimensional by ANSYS Fluent 19.2. About mechanism of the combustion, detailed chemical kinetics [21] consisting of 9 species and 20 reversible elementary reactions used for the H_2-air combustion mechanism.

Table 1: Thermal properties of wall materials

Material	k_s (w/m.K)	ϵ
Quartz[12]	1.05	0.92
Silicon Carbide[22]	32.8	0.9

Solver Validation and Gride Study

A prototype MTPV power generator of Yang et al. [23], containing several stepped microtubes, differentiated by their wall thickness is selected for solver validation. Experimental results exist for the average wall temperature of the micro combustion chambers for premixed H_2-air combustion. The thickness of 0.6 mm is selected for comparison, and numerical results showed good agreement with the experimental results according to Figure 2.

Four different structured grides were generated for gride study. In order to extract the results in a better way, three guidelines have been defined and plotted according to Figure 3. AB is a polyline defined along the center of the microchannel width, CD and EF are straight lines on the top and bottom of the outer walls, respectively. Gride study is performed for the case of U=8 m/s, ϕ=0.8, b=6, a=0.5 mm and K= 1.05 W/m.K. Temperature values along the AB polyline are drawn for the grides. According to Figure 4, the dependency of the results on the grides can be ignorable for the gride containing 26100 cells. Therefore, the gride of 26100 cells is chosen for the rest of the results.

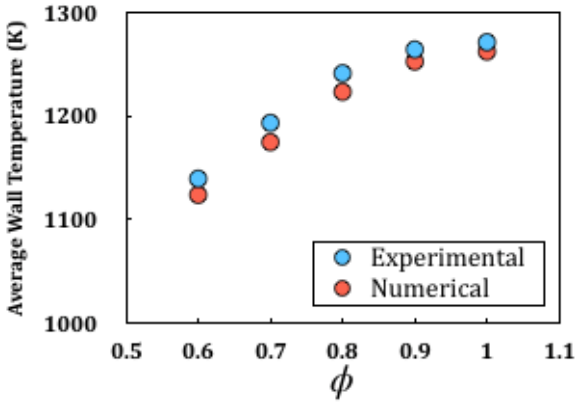

Figure 2: Solver validation for U=12 m/s and wall thickness of 0.6 mm

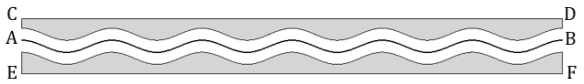

Figure 3: Defined guidelines for result extraction

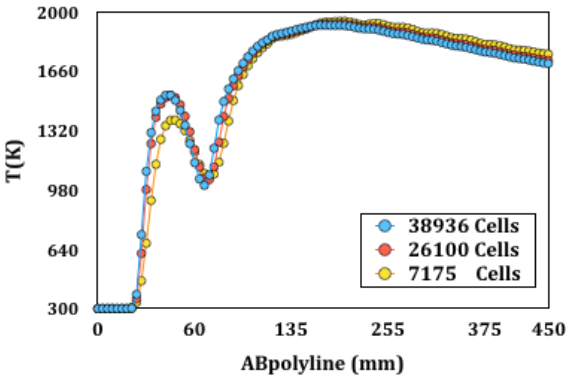

Figure 4: Temperature variations along the AB polyline for the case of U=8 m/s, ϕ=0.8, b=6, a=0.5mm and k_S = 1.05 W/m.K

Results and Discussion

Effect of Inlet Velocity

Results are presented in this section. The equivalence ratio was set to 0.8 for all cases. Since OH radical is an active radical in the flame front, it is elected to display the flame shape and location. Thus, contours of OH mass fraction are shown in Figure 5 for the case of b=6, a=0.2 mm, and K= 1.05 W/m.K versus various inlet velocities. According to the contours, the flame has an asymmetric shape at all considered velocities due to the asymmetric geometry of the microchannel. Also, the flame is strengthened near the walls because the OH mass fraction has a higher value. The reason is the existence of concave areas in the walls which operate as cavities and cause to reduce flow velocity. Therefore, flow residence time increases versus reaction time near the walls. Subsequently, the released heat of combustion should be more significant in the concave areas.

As shown in the Figure 5, flame stretch increases, as the inlet velocity increases. While inlet velocity enhancement has no considerable effect on the flame location (near the walls) from the beginning of the channel even when the inlet velocity increases up to 16 m/s. Therefore, wavy walls can prevent blow-out at high inlet velocities and increase the upper flammability limit because they fix the flame at the inlet.

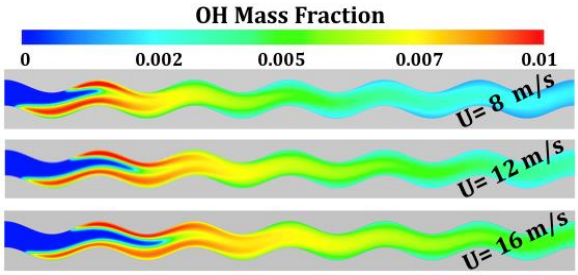

Figure 5: OH mass fraction variation for various inlet velocities, b=6, a=0.5 mm, ϕ=0.8 and k_S = 1.05 W/m.K

Figures 6 (a)-(c) show temperature distribution versus the inlet velocities along the defined guidelines. It is observed in Figure 6 (a) that reacting flow has a higher temperature in the first half of the microchannel at lower inlet velocities. In contrast, it has a lower temperature in the second half of the channel because the combustion zone moves from the centerline to the concave areas of the wall by inlet velocity enhancement, according to the Figure 5. Inlet velocity enhancement decreases flow residence time versus diffusion time across the fluid flow. Therefore, released heat of combustion and species need a longer distance to diffusion from the near walls (where generated) to the center of the microchannel. That's why the flow has a lower temperature along the first half of the centerline. However, flame stretch increment at high inlet velocity makes the reacting flow have a higher temperature at higher inlet velocities in the second half of the microchannel, according to Figure 6 (a). Figures 6 (b) and (c) illustrate temperature variation along the top and bottom walls, respectively.

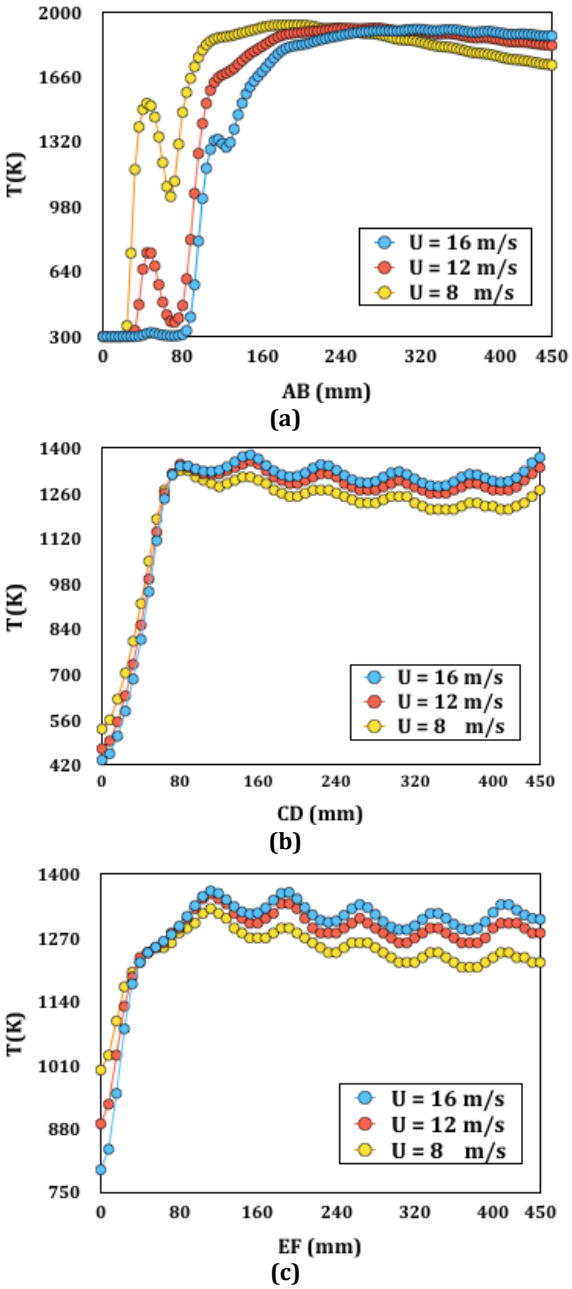

Figure 6: Temperature variation versus inlet velocity along the defined guidelines for (a) fluid, (b) upper wall and (c) bottom wall for ϕ=0.8, b=6, a=0.5 mm and k_S = 1.05 W/m.K.

According to the figures, the bottom wall has a higher temperature near the inlet because the first concave area of the bottom wall is closer to the inlet. Wall temperature increases with the inlet velocity at the rest of the length due to the flame stretch and other concave areas. The flame surface increases, as the flame stretch. It causes to increase released heat of combustion. Moreover, inlet velocity enhancement causes to push the combustion zone to the walls. Therefore, most of the combustion heat is released near the wall. Due to the lower value of the flow velocity, especially in the concave areas, there is more time to transfer the heat of combustion to the

walls than the center of the channel. Therefore, wall temperature increases with the inlet velocity.

Effect of the Wave's number

The parameter b denotes the number of concave areas named as concave or wave number. Effect of wave number on the combustion zone shown in Figure 7 for the case of a = 0.5 mm, U = 16 m/s and K = 1.05 W/m.K. According to the figure, as the number of waves increases, concave areas become smaller and closer to the inlet. Therefore, trapped combustion zones in the concaves are closer to the inlet. Consequently, flame stabilizes at the beginning of the microchannel even if the inlet velocity enhances up to 16 m/s. Figures 8 (a) and (b) represent upper and bottom wall temperature distribution versus various wave numbers, respectively. As the Figure 8 (a) indicates, upper wall temperature increases with the wave number, especially in the vicinity of the inlet because concave areas locate closer to the inlet. In addition, the number of trapped combustion zones increases in the vicinity of the inlet.

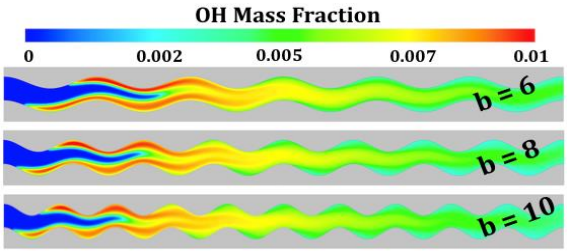

Figure 7: Effect of the wall wave number on the flame, U=16m/s, a=0.5 mm, ϕ=0.8 and K=1.05W/m.K.

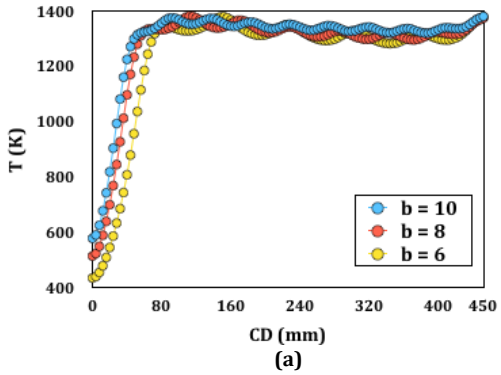

(a)

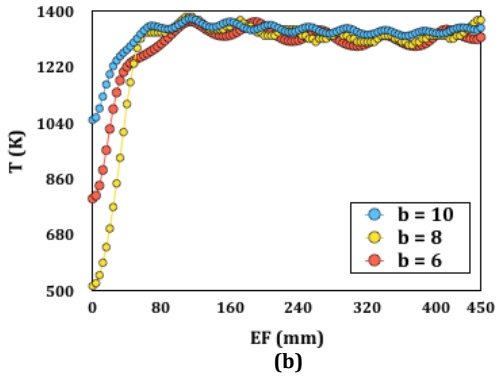

(b)

Figure 8: Temperature variation versus different wave numbers for (a) upper wall and (b) bottom wall at ϕ=0.8, U=16m/s, a=0.5 mm and k_S=1.05W/m.K.

Effect of concave number enhancement on the wall temperature enhancement is greater for the bottom wall, according to the Figure 8 (b). As the wave number increases from 6 to 10, wall temperature raises by 534 K in the vicinity of the inlet. This is desirable for MTPV applications where high and uniform wall temperature distribution is needed for the emitter efficiency enhancement.

Therefore, as the wave number increases and subsequently concave areas become more, especially in the vicinity of the inlet, wall temperature becomes higher and more uniform.

Effect of the wave's amplitude

Three microchannels that are differentiated by their wall's wave amplitude are investigated in this section. Contours of OH mass fraction shown in Figure 9 for U = 12 m/s and K = 1.05 W/m.K. The case a = 0 belongs to the microchannel without wavy walls or flat microchannel. According to the figure, flame locates at the middle of the flat microchannel and has an asymmetric shape. The reason may be the production and consumption of species with different molecular mass and mass diffusion coefficients during the combustion process. Each species related to its diffusive velocity and molecular mass, has different diffusive momentum. Collision of these species causes to change in the direction of the diffusive momentum vectors. It causes the flame to become asymmetric in some cases [24].

Making waves in the walls causes the flame to move toward the inlet to survive and intensify in the concave areas. Figures 10 (a)-(c) show temperature distribution along the defined guidelines for different values of wave amplitude at the inlet velocity of 12 m/s. According to the Figure 10 (a), for the flat microchannel, flow temperature remains 300 K up to slightly more than a third of the channel. While it has a maximum value than the other microchannels at the last third of the channel. Because the flame belongs to the flat microchannel placed ahead of the others.

Increasing the wave's amplitude increases the fluid temperature at the upstream due to flame formation in the concaves near the inlet. As the wall's amplitude increases, wall temperature increases in the first half of the microchannel. By increasing the wave's amplitude from 0.2 mm to 0.5 mm, wall temperature increases about 175 K at the inlet. Wall temperature remains lower than the others in most of the wall for the flat microchannel. Because most of the heat releases in the middle of the channel, according to the Figure 10 (a), whereas in the wavy microchannels most of the heat releases in the vicinity of the walls and inlet due to the existence of concave areas. It causes heat transfer from the hot flue gas to the wall to perform better. Because the surface of heat transfer increases due to waves of the inner walls. In addition, flow velocity in the vicinity of the wall is lower than the center. Therefore, the

released heat of combustion has more time to transfer from flue gas to the wall.

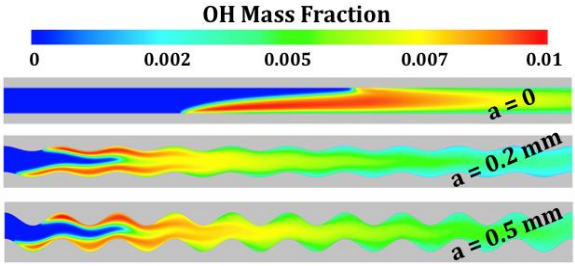

Figure 9: OH mass fraction variation for various wall's wave amplitudes, U=12m/s, ϕ=0.8, and k_S=1.05 W/m.K.

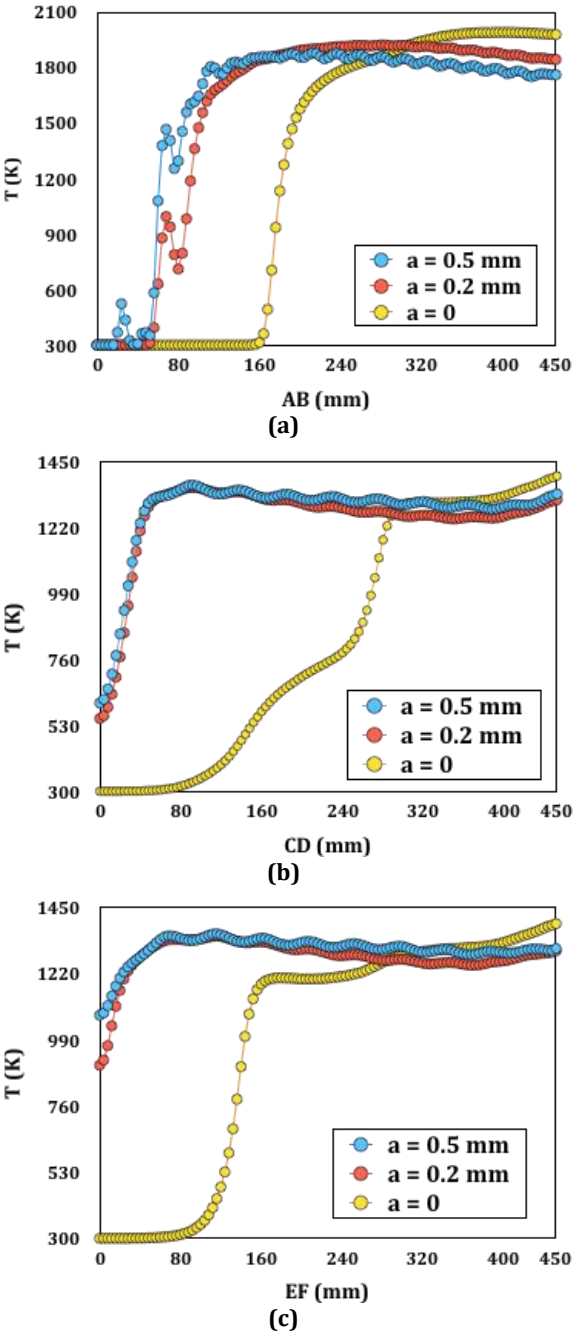

Figure 10: Temperature variation versus different wall's wave amplitudes for (a) fluid, (b) upper wall and (c) bottom wall for ϕ=0.8, U=12m/s and k_S=1.05 W/m.K.

Effect of the Wall Thermal Conductivity

Since the wall thickness and hydraulic diameter have the same order of magnitude in microchannels, heat transfer through the wall significantly affects the self-sustaining of the combustion and combustion characteristics. Wall can promote combustion stability and make sustainable combustion by conducting heat of combustion from downstream to upstream or heat recirculation. On the other hand, when the rate of heat recirculation becomes much higher in the way that causes to unbalance between the rate of released heat and the rate of heat transfer to the wall, the flame becomes unsteady or extinguishes. With this in mind, two materials with different thermal conductivity and almost equal thermal radiation emissivity are considered for the investigation role of the wall material, according to the Table 1. Temperature variation along the walls shown in Figure 11 versus different values of wall thermal conductivity for inlet velocity of 16 m/s. As illustrated in the figure, thermal conductivity enhancement disappears wall temperature fluctuations. Also, wall temperature increases and becomes more uniform with the enhancement of thermal conductivity. As the thermal conductivity increases up to 32.08 W/m.K, upper and bottom wall temperatures rise to 567 K and 286 K, respectively. It means that heat recirculation has better done. Therefore, wall thermal conductivity enhancement up to 32.08 w/m.K is beneficial for wavy walls from the viewpoint of heat recirculation.

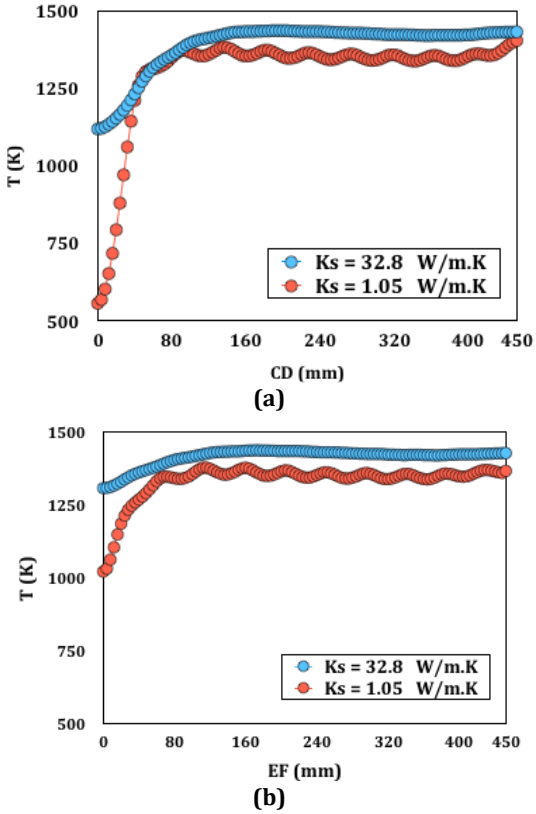

Figure 11: Temperature variation for different wall thermal conductivities plotted along the (a) upper wall and (b) bottom wall for ϕ=0.8, U=16m/s, b=10, and a=0.5 mm

Investigation of Efficiency for MTPV Application

In this section, introduced parameters in the Eqs. (14)-(19) with the average values of temperatures are calculated in Table 2. Both the upper and bottom walls are exposed to PV cells and calculations of the Table 2 are performed for both of upper and bottom outer surfaces. Calculations performed per unit length of micro combustor's depth. Maximum and minimum values in each column of the table are bolded. According to the table, the rate of released heat increases with the inlet velocity. Because hydrogen mass flow rate increases. Also, the radiation heat transfer rate and overall heat transfer rate are increased, as the inlet velocity increases up to 16 m/s. Because the average wall temperature increases due to flame transfer towards the wall and flame stretch. While the average fluid temperature decreases because of heat transfer enhancement between the fluid and wall.

Although the average wall temperature increases, emitter and total efficiency of the system are reduced. It means that the system has lower efficiency despite higher wall temperature. That is because the rate of released heat increases two times, as the inlet velocity becomes double. While $\dot{Q}_{Rad}$ and $\dot{Q}_{w}$ increase just 18.83% and 17.84%, respectively. Therefore, emitter and total efficiency decrease with the inlet velocity because the emitter efficiency enhancement is not so great to dominate energy conversion efficiency enhancement.

$\dot{Q}_{R}$ remains constant with the wave number variation, whereas emitter and total efficiency are increased. Because the heat transfer rate to the wall increases due to surface enhancement. For the flat microchannel, efficiencies have lower values. Because most of the heat releases in the center and the flame locates at the middle of the channel due to the lack of concave areas. According to the results, the wave's amplitude increment from 0.2 mm to 0.5 mm has no considerable effect on the efficiencies. While the total efficiency of the wavy wall microchannel (b=10 and a=0.2 mm) is 74% higher that the flat wall microchannel.

Wall thermal conductivity enhancement leads to an increase $\dot{Q}_{Rad}$ about 28%, whereas $\dot{Q}_{R}$ remains constant. Therefore, the total efficiency of the system rises about 28%. Also, wall average temperature increases because temperature distribution becomes uniform due to heat recirculation enhancement. Therefore, using Silicon Carbide for wall material is more beneficial than Quartz.

Conclusion

Combustion characteristics of premixed H_2-air numerically investigated in various wavy wall microchannels to determine the feasibility and performance of such geometries for usage as the emitter in the MTPV systems. Results showed that wall temperature increases by inlet velocity enhancement due to flame transfer towards the concave areas where the combustion zone releases most of the heat in the vicinity of the wall. Therefore, wall temperature increases, whereas the total efficiency of the MTPV system decreases because the effect of the inlet velocity enhancement on the released heat of combustion is more severe than the wall thermal radiation.

As the wave number increases, the flame moves towards the inlet even when the inlet velocity increases up to 16 m/s. Therefore, wavy wall microchannels showed a higher upper flammability limit. Wall wave number impacts the efficiency and wall average temperature, and both increase with the wall's wave number. In comparison with the similar flat wall microchannel, the total efficiency of the wavy wall microchannel increased up to 74%, as the wave number and wall's wave amplitude enhanced to 10 and 0.2 mm, respectively. From the viewpoint of wall material, Silicon carbide has better thermal performance than Quartz. Because of better heat recirculation due to higher thermal conductivity while equal thermal radiation emissivity.

Table 2: Calculated parameters related to the performance of the MTPV system

	$\dot{Q}_R$(W/m)	$\dot{Q}_{Rad}$(W/m)	$\dot{Q}_w$(W/m)	η_Q(%)	η_{Rad}(%)	η_{total}(%)	$T_{avg,F}$(K)	$T_{avg,W}$(K)	$T_{avg,CD}$(K)	$T_{avg,EF}$(K)
U(m/s)				**φ=0.8, b=6, a=0.5 mm and k_S =1.05 W/m.K**						
8	**38818.94**	10896.96	11724.69	**30.20**	**28.07**	**4.21**	**1636**	1225	1202	1247
12	58228.41	12236.56	13091.58	22.4	21	3.15	1618	1256	1232	1280
16	77637.88	12949.8	13816.88	17.79	16.68	2.5	1582	1263	1245	1295
b				**U = 16m/s, φ=0.8, a=0.5mm and k_S =1.05 W/m.K**						
6	77637.88	12949.8	13816.88	17.79	16.68	2.5	1582	1263	1245	1295
8	77637.88	13605	14495.82	18.67	17.5	2.62	1606	1290	1279	1314
10	77637.88	14323.95	15233.73	19.62	18.45	2.77	1631	1311	1304	1333
a(mm)				**U = 12m/s, φ=0.8, b=10 and k_S =1.05 W/m.K**						
0	58228.41	**7187.22**	**7734.98**	**13.28**	**12.34**	**1.85**	**1180**	**909**	**987**	**834**
0.2	58228.41	12520.95	13390.14	23	21.5	3.22	1631	1266	1257	1285
0.5	58228.41	12236.56	13091.58	22.4	21	3.15	1618	1256	1232	1280
k_S (W/m.K)				**U = 16m/s, φ=0.8, b=10 and a=0.5mm**						
1.05	77637.88	14323.95	15233.73	19.62	18.45	2.77	1631	1311	1304	1333
32.8	77637.88	**18317.2**	**19309.4**	24.87	23.6	3.54	1602	**1402**	**1390**	**1415**

List of Symbols

a	wall's wave amplitude(mm)
b	wave number
C_1	Constant
C_2	Constant
$C_{1\varepsilon}$	Constant
$C_{2\varepsilon}$	Constant
$C_{3\varepsilon}$	Constant
D_{ij}	Binary diffusion coefficient of the i^{th} species in j^{th} species (m^2/s)
$D_{i,m}$	Average diffusivity of the i^{th} species in the mixture (m^2/s)
G_k	Generation of the turbulence kinetic energy due to the mean velocity gradient
G_b	Generation of the turbulence kinetic energy due to the buoyancy
h	Enthalpy of the mixture (J/kg)
h_{conv}	External thermal convection coefficient ($W/m^2.K$)
h_i	Enthalpy of the i^{th} species (J/kg)
k	Turbulence kinetic energy rate
K_f	Fluid thermal conductivity (W/m.K)
k_B	Boltzmann constant, 1.381×10^{-23} (J/K)
k_S	Wall thermal conductivity (W/m.K)
$\dot{m}$	Mass flow rate (kg/m^3)
P	Pressure (pa)
$\dot{Q}_{LHV}$	Lower heating value (MJ/Kg)
$\dot{Q}_R$	Chemical heat release rate
$\dot{Q}_{Rad}$	Radiation heat transfer rate from the external surfaces
$\dot{Q}_w$	Total heat transfer rate from the external wall
R_u	Universal Gas constant (J/Kg. K)
S_k	User defined source term
S_ε	User defined source term
T	Temperature (K)
$T_{avg,CD}$	Average temperature along CD guideline (K)
$T_{avg,EF}$	Average temperature along EF guideline (K)
$T_{avg,F}$	Average temperature of fluid (K)
$T_{avg,W}$	Average temperature of wall (K)
u	Velocity vector (m/s)
U	Velocity magnitude (m/s)
$\overline{W}$	Mean molecular weight of the mixture
W_{ij}	Mean molecular weight of i^{th} and j^{th} species
x	Mole fraction
Y	Mass fraction
Y_M	Contribution of the fluctuating dilatation in compressible turbulence to the overall dissipation rate
ρ	Density (Kg/m^3)
μ	Dynamic viscosity of the mixture (kg/m.sec)
μ_t	Turbulent viscosity
Ω_D	Collision integral
$\overline{\Omega}_{ij}$	Mean rate of rotation tensor
ϵ	Thermal radiation emissivity of surface
ε	Kinetic energy dissipation rate
ε_i	Lennard-Jones energy of the i^{th} species
ω_k	Angular velocity
$\dot{\omega}_i$	Rate of reaction of the i^{th} species ($kg/m^3.sec$)
σ	Stefan-Boltzmann constant, $5.67\times10^{-8}\ W/m^2.K^4$
σ_i	Collision diameter (Å)
σ_{ij}	Mean collision diameter of the i^{th} and j^{th} species (Å)
σ_k	Turbulent Prandtl number for k
η_{MTPV}	Total energy conversion efficiency of the MTPV system
η_Q	Energy conversion efficiency (%)
η_{Rad}	Emitter efficiency (%)
η_{total}	Total energy conversion efficiency of the MTPV system (%)
δ_{ij}	Kronecker delta matrix
ϕ	Equivalence ratio
v	Kinematic viscosity (m^2/s)

References

[1] D. S. S Ishizuka, D Dunn-Rankin, R W Pitz, R J Kee, Y Zhang, H Zhu, T Takeno, M Nishioka, *Tubular Combustion*. New York: Momentum Press, 2013.

[2] W. M. Yang, S. K. Chou, C. Shu, H. Xue, and Z. W. Li, "Development of a prototype micro-thermophotovoltaic power," *J. Phys. D. Appl. Phys.*, vol. 37, pp. 1017–1020, 2004, doi: 10.1088/0022-3727/37/7/011.

[3] W. M. Yang, S. K. Chou, C. Shu, Z. W. Li, and H. Xue, "Experimental study of micro-thermophotovoltaic systems with different combustor configurations," *Energy Convers. Manag.*, vol. 48, no. 4, pp. 1238–1244, 2007, doi: 10.1016/j.enconman.2006.10.002.

[4] J. Li, S. K. Chou, G. Huang, W. M. Yang, and Z. W. Li, "Study on premixed combustion in cylindrical micro combustors: Transient flame behavior and wall heat flux," *Exp. Therm. Fluid Sci.*, vol. 33, no. 4, pp. 764–773, Apr. 2009, doi: 10.1016/j.expthermflusci.2009.01.012.

[5] A. Fan, J. Wan, K. Maruta, H. Yao, and W. Liu, "Interactions between heat transfer, flow field and flame stabilization in a micro-combustor with a bluff body," *Int. J. Heat Mass Transf.*, vol. 66, pp. 72–79, 2013, doi: 10.1016/j.ijheatmasstransfer.2013.07.024.

[6] A. Fan, J. Wan, Y. Liu, B. Pi, H. Yao, and W. Liu, "Effect of bluff body shape on the blow-off limit of hydrogen/air flame in a planar micro-combustor," *Appl. Therm. Eng.*, vol. 62, no. 1, pp. 13–19, 2014, doi: 10.1016/j.applthermaleng.2013.09.010.

[7] M. Ansari and E. Amani, "Micro-combustor performance enhancement using a novel combined baffle-bluff configuration," *Chem. Eng. Sci.*, vol. 175, pp. 243–256, 2018, doi: 10.1016/j.ces.2017.10.001.

[8] S. Akhtar, J. C. Kurnia, and T. Shamim, "A three-dimensional computational model of H2-air premixed combustion in non-circular micro-channels for a thermo-photovoltaic (TPV) application," *Appl. Energy*, vol. 152, pp. 47–57, Aug. 2015, doi: 10.1016/j.apenergy.2015.04.068.

[9] P. Qian *et al.*, "Effects of bluff-body on the thermal performance of micro thermophotovoltaic system based on porous media combustion," *Appl. Therm. Eng.*, vol. 174, no. April, p. 115281, 2020, doi:

10.1016/j.applthermaleng.2020.115281.

[10] W. Zuo, Y. Zhang, Q. Li, J. Li, and Z. He, "Numerical investigations on hydrogen-fueled micro-cylindrical combustors with cavity for micro-thermophotovoltaic applications," *Energy*, vol. 223, p. 120098, 2021, doi: 10.1016/j.energy.2021.120098.

[11] A. Alipoor, A. Kadkhoda, and P. Abbaspour, "Combustion characteristics of hydrogen-air mixture in a radial micro combustor for using in thermophotovoltaic devices," *Int. J. Energy Res.*, no. March, pp. 1–20, 2021, doi: 10.1002/er.6692.

[12] W. Zuo, E. Jiaqiang, D. Han, and Y. Jin, "Numerical investigations on thermal performance of double-layer four-channel micro combustors for micro-thermophotovoltaic system," *Energy Convers. Manag.*, vol. 150, pp. 343–355, Oct. 2017, doi: 10.1016/j.enconman.2017.08.029.

[13] A. Alipoor and M. H. Saidi, "Numerical study of hydrogen-air combustion characteristics in a novel micro-thermophotovoltaic power generator," *Appl. Energy*, vol. 199, 2017, doi: 10.1016/j.apenergy.2017.05.027.

[14] E. Nadimi and S. Jafarmadar, "The numerical study of the energy and exergy efficiencies of the micro-combustor by the internal micro-fin for thermophotovoltaic systems," *J. Clean. Prod.*, vol. 235, pp. 394–403, 2019, doi: 10.1016/j.jclepro.2019.06.303.

[15] Z. He *et al.*, "Numerical investigation on a multi-channel micro combustor fueled with hydrogen for a micro-thermophotovoltaic system," *Int. J. Hydrogen Energy*, vol. 46, no. 5, pp. 4460–4471, 2021, doi: 10.1016/j.ijhydene.2020.10.160.

[16] Z. Mansouri, "Combustion in wavy micro-channels for thermo-photovoltaic applications – Part I: Effects of wavy wall geometry, wall temperature profile and reaction mechanism," *Energy Convers. Manag.*, vol. 198, Oct. 2019, doi: 10.1016/j.enconman.2018.12.105.

[17] Z. Mansouri, "A novel wavy micro-combustor for micro-thermophotovoltaic applications," *Chem. Eng. Process. - Process Intensif.*, vol. 163, no. March, p. 108371, 2021, doi: 10.1016/j.cep.2021.108371.

[18] H. Yilmaz, O. Cam, S. Tangoz, and I. Yilmaz, "Effect of different turbulence models on combustion and emission characteristics of hydrogen/air flames," *Int. J. Hydrogen Energy*, vol. 42, no. 40, pp. 25744–25755, 2017, doi: 10.1016/j.ijhydene.2017.04.080.

[19] S. R. Turns, *An Introduction to Combustion Concepts and Applications*. McGraw-Hill, 2012.

[20] X. Yang, L. Zhao, Z. He, S. Dong, and H. Tan, "Comparative study of combustion and thermal performance in a swirling micro combustor under premixed and non-premixed modes," *Appl. Therm. Eng.*, vol. 160, no. March, p. 114110, 2019, doi: 10.1016/j.applthermaleng.2019.114110.

[21] P. W. J. Marinov N. M, Westbrook C. K, "Detailed and global chemical kinetics model for hydrogen," in *Conference: 8. international symposium on transport properties, San Francisco, CA (United States)*, 1995, [Online]. Available: https://www.osti.gov/biblio/90098.

[22] W. Zuo, E. Jiaqiang, Q. Peng, X. Zhao, and Z. Zhang, "Numerical investigations on thermal performance of a micro-cylindrical combustor with gradually reduced wall thickness," *Appl. Therm. Eng.*, vol. 113, pp. 1011–1020, 2017, doi: 10.1016/j.applthermaleng.2016.11.074.

[23] Y. Wenming, C. Siawkiang, S. Chang, X. Hong, and L. Zhiwang, "Effect of wall thickness of micro-combustor on the performance of micro-thermophotovoltaic power generators," *Sensors Actuators, A Phys.*, vol. 119, no. 2, pp. 441–445, 2005, doi: 10.1016/j.sna.2004.10.005.

[24] P. Abbaspour and A. Alipoor, "Numerical study of combustion characteristics and oscillating behaviors of hydrogen – air combustion in converging – diverging microtubes," *Int. J. Heat Mass Transf.*, vol. 159, pp. 120127, 2020, doi: 10.1016/j.ijheatmasstransfer.2020.120127.